Journal of the Indian Chemical Society 103 (2026) 102406

Contents lists available at ScienceDirect

Journal of the Indian Chemical Society

journal homepage: www.journals.elsevier.com/journal-of-the-indian-chemical-society

Core–shell Silica–Ruthenium hexacyanoferrate nanoparticles modified electrode as efficient electrocatalyst for riboflavin detection and oxygen evolution reaction

S. Anuja [a,*], J.A.F.C.R. Rodrigues [b], R. Suresh Babu [b,**], A. Kosiha [c], A.L.F. de Barros [b]

[a] Department of Chemistry, Loyola College, Chennai, 600 034, Tamil Nadu, India
[b] Laboratory of Experimental and Applied Physics, Centro Federal de Educação Tecnológica Celso Suckow da Fonseca, Av. Maracanã 229, Rio de Janeiro, 20271-110, Brazil
[c] Department of Chemistry, Vels Institute of Science, Technology & Advanced Studies (Deemed to be University), Chennai, 600 117, India

ARTICLE INFO

Keywords:
Core-shell
Silica
Riboflavin
Metal hexacyanoferrate
OER

ABSTRACT

An innovative core–shell nanoparticle system comprising a silica (SiO_2) core and a ruthenium hexacyanoferrate (RuHCF) shell was successfully synthesized. The structural and optical behaviour of the resulting SiO_2@RuHCF nanoparticles (NPs) were characterized by UV–visible spectroscopy. The surface morphology and nanoscale architecture were further elucidated through field-emission scanning electron microscopy (FESEM) and high-resolution transmission electron microscopy (HRTEM), confirming the successful encapsulation of RuHCF on the silica core. The electrochemical functionality of the synthesized SiO_2@RuHCF-NPs was explored by incorporating them into a paraffin wax-impregnated graphite electrode (PIGE) via mechanical immobilization, forming an electroactive redox mediator system. The modified electrode was characterized by voltammetric methods and demonstrated excellent electrocatalytic activity toward the riboflavin reduction. The developed riboflavin sensor exhibited a fast response time of 4 s, a low detection limit of 1.4×10^{-7} M, a broad linear range of 4.3–2600 μM, high sensitivity 0.204 μA/μM, and showed good stability and repeatability. These features highlight the sensor's potential for practical applications. Furthermore, the modified electrode also facilitated oxygen evolution in alkaline medium, achieving an optimal current density of 10 mA cm^{-2} at overpotential of just 560 mV from the thermodynamic potential of 1.23 V, indicating its promise for electrocatalytic applications.

1. Introduction

Core–shell nanoparticles have emerged as a prominent class of materials at the intersection of chemistry, electronics, biomedicine, optics, and catalysis. Their tunable mechanical, optical, electrical, magnetic, and catalytic properties can be precisely controlled by altering the core and shell composition or their ratio [1]. Particularly, systems comprising inexpensive cores and reactive shells have attracted significant interest due to their combined functional performance and economic efficiency. Structuring reactive materials as thin shells on low-cost cores minimizes the use of valuable materials while enhancing activity through core-induced strain and ligand effects [2]. This design strategy not only improves material properties but also reduces the consumption of precious components, offering a cost-effective alternative to bulk or pure nanomaterials [3].

Silica (SiO_2) is widely used as a core material in non-magnetic particles due to its remarkable resistance to coagulation. This resistance stems from its extremely low Hamaker constant, which determines the van der Waals attractive forces between the particles and the surrounding medium [4]. Additionally, silica is chemically stable, optically transparent, and does not interfere with redox processes at the particle core. To ensure particles stay uniformly dispersed in the medium, it is often necessary to coat them with a suitable encapsulating shell [5]. Recently, metal hexacyanoferrates (MHCFs) are a class of coordination complex consisting of transition metal-ions coordinated to hexacyanoferrate ligands, typically having a general formula like $M_3[Fe(CN)_6]_2$ or $M[Fe(CN)_6]$, where M represents a transition metal such as Cu, Co, Ni, or Ru. These materials belong to the broader family of

* Corresponding author.
** Corresponding author.
E-mail addresses: dranuja@loyolacollege.edu (S. Anuja), suresh.rajendran@aluno.cefet-rj.br (R. Suresh Babu).

https://doi.org/10.1016/j.jics.2026.102406
Received 18 August 2025; Received in revised form 15 December 2025; Accepted 2 January 2026
Available online 3 January 2026

Prussian Blue and its analogues [6]. MHCFs are particularly attractive in electrochemical applications due to several key features such as fast and reversible redox behaviour, insolubility in redox states, tunable electrochemical properties and selective ion-exchange capability [7].

Nutritional elements like vitamins tend to deteriorate during processing, storage, and preservation. These degradations occur due to changes in environmental factors such as pH, temperature, and humidity. To evaluate the extent of nutrient degradation during production and storage, there is a growing demand for quick, cost-effective, and straightforward methods for accurately determining micronutrient levels [8]. Riboflavin (vitamin B_2) is a crucial dietary and pharmaceutical component, playing a significant role in cellular respiration and energy production from carbohydrates, fats, and acids. It is widely present in most natural food sources. Typically, a daily loss of 30 μg of riboflavin per gram of creatinine or lower is an indicator of deficiency, which may result in conditions like angular stomatitis and cheilosis [9]. Consequently, it is important to monitor its levels, and various analytical approaches have been developed for this purpose. These include techniques such as liquid chromatography [10], chemiluminescence [11], spectroelectrochemistry [12], and fluorescence [13]. Nonetheless, these techniques are often laborious, time-intensive, and require complex protocols and costly instruments. Owing to their high sensitivity and selectivity, electrochemical methods have been employed for detecting trace levels of riboflavin in food samples and pharmaceutical formulations—even in the presence of significant quantities of interfering substances [14].

Water splitting has garnered significant consideration in the area of energy storage and conversion due to the ease of hydrogen production and its environmentally friendly nature [15–17]. The overall water splitting process involves two half-reactions: the hydrogen evolution reaction (HER, $2H_2O + 2e^- \rightarrow H_2 + 2OH^-$) occurring at the cathode, and the oxygen evolution reaction (OER, $4OH^- \rightarrow O_2 + 2H_2O + 4e^-$) at the anode [18,19]. While both half-reactions contribute to the overall efficiency of electrochemical water splitting, large-scale hydrogen production is predominantly limited by the OER [20,21]. This anodic reaction is intrinsically sluggish due to its complex four-electron transfer mechanism, necessitating a higher overpotential than the theoretical 1.23 V required for water decomposition [22,23]. This leads to excessive energy consumption in practical applications. To address this challenge, the development of cost-effective catalysts with excellent electrocatalytic performance—characterized by higher current density and lower overpotentials—is essential. Currently, noble-metal oxides for example RuO_2 and IrO_2 are considered benchmark OER catalysts due to their superior activity. However, their widespread commercial application is hindered by high costs and limited availability [24,25]. Consequently, extensive research has been directed toward alternative materials, particularly transition metal-based compounds including oxides, layered hydroxides, alloys, chalcogenides and coordination complexes. These materials offer advantages such as natural abundance, mixed valence states, and strong intrinsic electroactivity, making them promising candidates for efficient and scalable OER catalysis [26–28].

To the best of our knowledge, this is the first report on the development of an electrochemical sensor for riboflavin detection using a novel SiO_2 core/RuHCF shell (SiO_2@RuHCF) modified electrode. Experimental results indicate that the proposed electrode significantly lowers the reduction potential of riboflavin. When differential pulse voltammetry is employed for precise quantification, the reduction current exhibits a linear relationship with riboflavin concentration in the range of 4.3–2600 μM, with a detection limit of approximately 1.4×10^{-7} M. Meanwhile, the proposed modified electrode can also effectively avoid the interferences and has been used to the determinations of riboflavin with higher sensitivity and excellent selectivity. These results, combined with the enhanced oxygen evolution reaction (OER) performance, underscore the multifunctional capabilities of the SiO_2@RuHCF-modified electrode and its potential for application in both energy conversion and biosensing platforms.

2. Experimental

2.1. Reagents and equipments

Tetraethyl orthosilicate (TEOS 98 % - reagent grade) and ruthenium chloride trihydrate ($RuCl_3.3H_2O$) were purchased from Sigma- Aldrich chemicals. Ammonia solution (30 % pure) and potassium ferricyanide (III) ($K_3[Fe(CN)_6]$) were obtained from Merck specialities Pvt. Ltd. and Riboflavin was from S.D. Fine chemicals. Spectroscopic grade graphite rod (3 mm dia.) was used as received from Aldrich. Distilled ethanol was used for the synthesis of nanoparticles and doubly distilled water was applied for the electrochemical studies.

The morphology of the nanoparticles was investigated by FESEM (Model: SU600, HITACHI, Japan) and HRTEM (Model: FEI, Tecnai G^2–model T-30 S-twin, with 300 kV). FESEM samples were prepared by dropping the colloidal suspension onto aluminium foils affixed with carbon conducting tape. HRTEM samples were prepared by depositing 5 μL of nanoparticle suspension (diluted 1:20) onto a 200-mesh copper grid with a carbon film backing. The electrochemical measurements were performed using a CHI 660B electrochemical workstation (CH Instruments, USA) with a conventional three-electrode setup. Modified and unmodified wax-impregnated graphite electrodes served as the working electrodes. A platinum wire was used as the counter electrode (CE), and a saturated calomel electrode (SCE) functioned as the reference electrode (RE). All potentials were recorded versus SCE, and all experiments were conducted at room temperature.

2.2. Synthesis of silica nanoparticles

The Stöber process, first reported in 1968 [29], enables the preparation of monodispersed SiO_2 colloids commonly known as “white carbon black” through the hydrolysis of alkyl silicates followed by the condensation of silicic acid in alcoholic solutions using ammonia as a catalyst. Since then, numerous research groups have employed these monodispersed silica colloids as model materials in a wide range of applications. Thus, this well-established method was used to synthesis silica nanoparticle (NP) with TEOS and solvent mixture (methanol, ethanol and water) by incorporating some minor modifications in the above method such as variation in methanol-ethanol mixture concentration (in the absence of water) and temperature. The condensation process involves the addition of 10 ml of TEOS (0.17 M) onto a stirred mixture of 100 mL methanol, 45 ml ethanol and 12 ml ammonia (0.8 M), continued stirring for 2 h at 55 °C.

2.3. Synthesis of SiO_2@RuHCF-NPs

The as prepared core-SiO_2 NPs were stirred for about 15 min with 10 mM HCl (10 mL) solution was added. This leads to the neutralization of anionic charges on the nanoparticle surface, resulting in the development of a positive surface charge. Stirring was then continued with 10 mL of 0.05 M $K_3[Fe(CN)_6]$ containing 10 mM HCl for 45 min. In the course of the reaction, positively charged SiO_2 surface adsorbs the negatively charged ferricyanide ion through electrostatic attraction. This was in par with literature for Fe_2O_3 NP [30]. Then, 10 mL of 0.05 M ruthenium chloride solution containing 10 mM HCl was added, and the resultant mixture was stirred for further 30 min. By this, a thin layer of RuHCF forms on the surface of SiO_2 NP as the nucleation centers which produces the core/shell nanostructure. The black-colored SiO_2@RuHCF nanoparticles formed were separated from the solution by centrifugation and washed with 10 mM HCl until the washings became colourless. They were then rinsed with redistilled water to neutralize, dried thoroughly, and stored under vacuum at room temperature.

2.4. Preparation of SiO_2@RuHCF-NPs modified electrode

A paraffin wax-impregnated graphite electrode (PIGE) with a

circular surface diameter of 3 mm, prepared as previously reported [31, 32], was used for electrode modification. One end of the electrode was carefully polished on a smooth surface using 0.5 μm alumina, rinsed with distilled water, and air-dried. The polished surface was then coated with SiO_2@RuHCF nanoparticles via mechanical transfer and employed as the working electrode.

3. Results and discussion

3.1. UV–vis studies of the SiO_2@RuHCF-NPs

A schematic representation for the preparation of core-shell SiO_2@RuHCF-NPs is shown in Scheme 1. The UV–Vis spectrum of both colloidal silica NP and silica coated with RuHCF-NPs in ethanol are shown in Fig. 1. Compared to the spectra of silica NP, SiO_2@RuHCF-NPs shows two peaks at 311 and 433 nm in ethanol. The spectra confirm the presence of RuHCF and are consistent with the earlier reports of ruthenium complex [33]. The sharp absorption peak at 311 nm can be assigned to the ligand to metal charge transfer (LMCT) band of $[Fe^{III}(CN)_6]$, and the metal centred peak at 433 nm is due to the MLCT transitions of Ru in RuHCF-NPs.

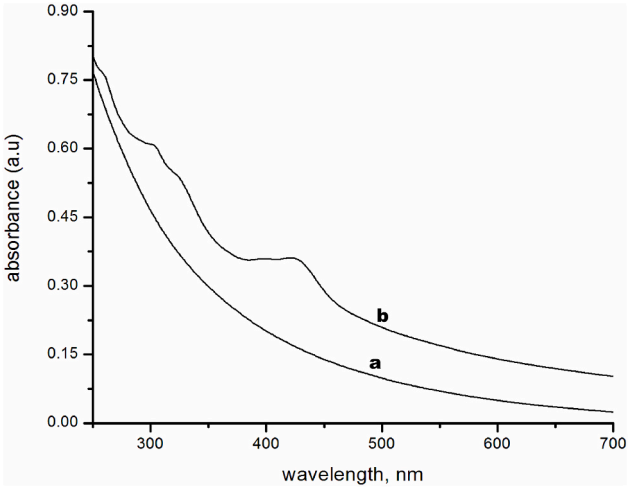

Fig. 1. UV–Visible spectra of (a) colloidal silica NP and (b) SiO_2@RuHCF-NPs in ethanol.

3.2. FESEM and HRTEM images of the SiO_2@RuHCF-NPs

The morphology study of the SiO_2@RuHCF-NPs was also studied by FESEM and is shown in Fig. 2A–C, which displays how they are present as core-shell nanocomposites. Images clearly expose the increase in diameter of the silica nanoparticles and how the inorganic polymer present as sheet over the colloidal silica nanoparticles (Fig. 2A) stepwise self-assembled with ferrocyanide (Fig. 2B) followed by RuHCF (Fig. 2C). The most common characterisation of core-shell nanoparticles is HRTEM, which gives a picture of silica core and it portrays the diameter of SiO_2 NP as 70–100 nm (Fig. 2D). It is interesting to find out that the ferrocyanide film seem to grow on the surface of spherical silica NP and the formation of the inorganic polymer, RuHCF as a shell over silica NP core is observed which is shown in Fig. 2E and F. The higher magnification clearly shows the presence of white shell over colloidal silica NP and no individual silica NP are found in the images confirms that the formation of core/shell nanomaterial is complete.

3.3. X-ray photoelectron spectroscopy analysis

X-ray photoelectron spectroscopy (XPS) was employed to confirm the elemental composition and oxidation states of the constituents in the synthesized core–shell nanoparticles. The survey spectrum (Fig. 3A) clearly exhibits distinct peaks corresponding to Si 2p, C 1s, N 1s, and O 1s, indicating the successful incorporation of these elements into the structure. These elements originate from the silica support, cyanide

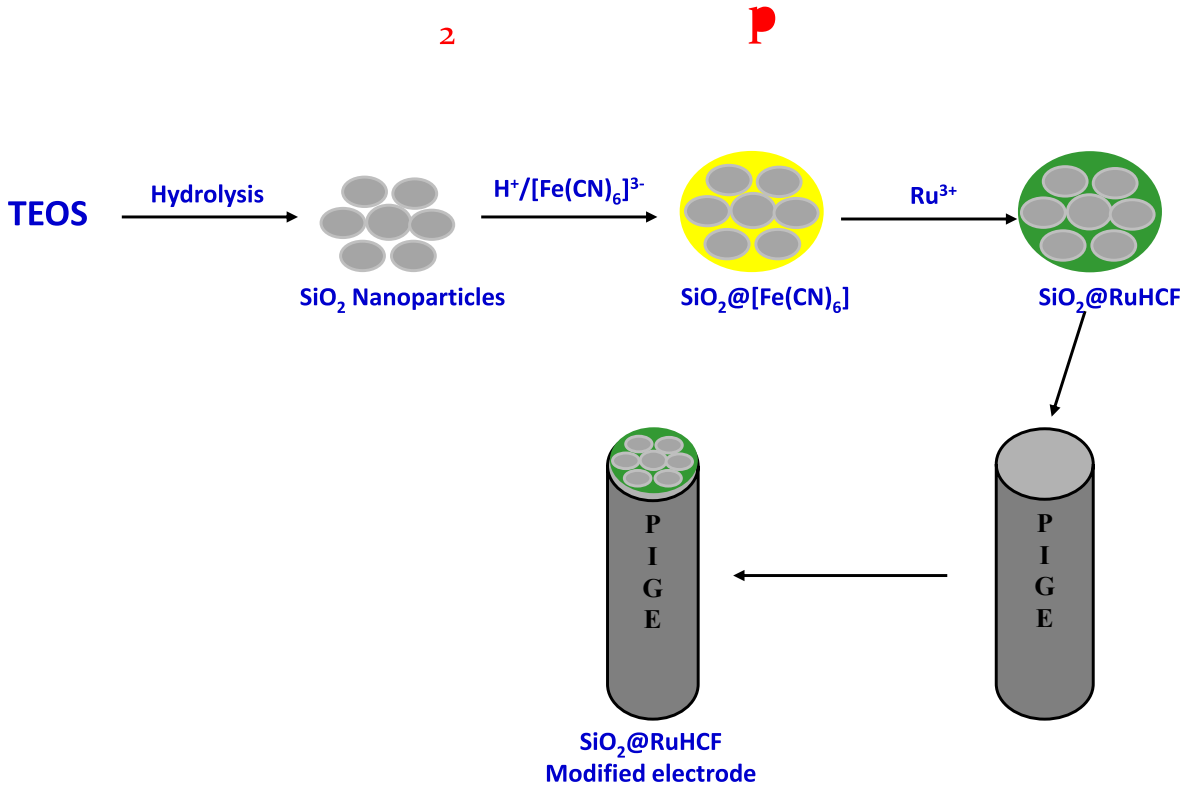

Scheme 1. Schematic representation for the preparation of core-shell SiO_2@RuHCF-NPs.

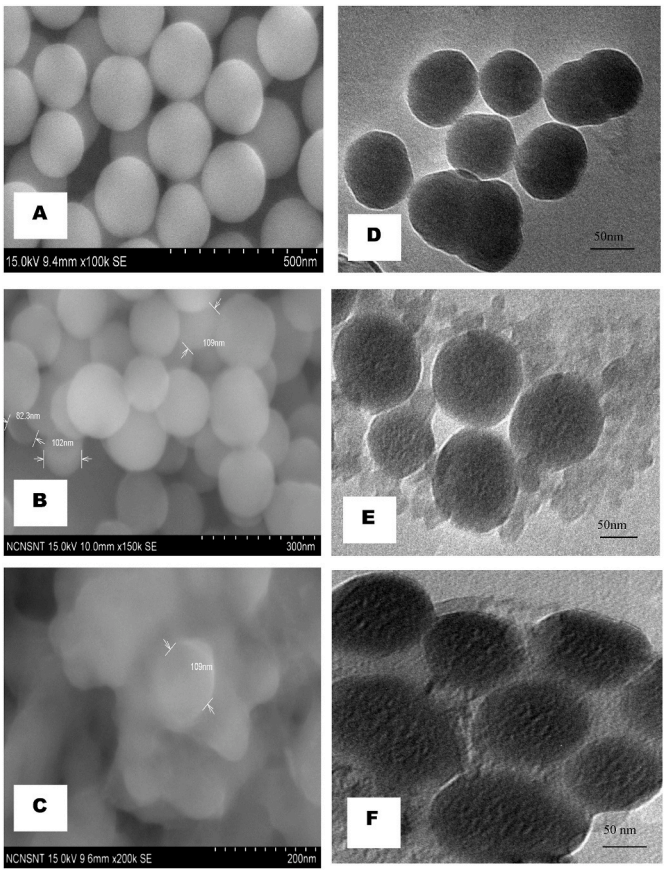

Fig. 2. FESEM and HRTEM images of (A & D) colloidal silica NP (B & E) ferrocyanide entrapping colloidal silica NP (C & F) Core-silica/Shell-RuHCF-NPs respectively.

ligands, and organic shell, respectively. To gain deeper insights into the oxidation states of the metal centers, high-resolution spectra of Fe and Ru were recorded. As shown in Fig. 3B, the Fe 2p region displays two prominent peaks at binding energies of 710.3 eV and 723.4 eV, corresponding to Fe $2p_{3/2}$ and Fe $2p_{1/2}$, respectively. The observed 2:1 intensity ratio is consistent with the spin–orbit splitting pattern of Fe^{3+} species. This strongly supports the presence of Fe^{3+} ions coordinated to cyanide ligands, as typically observed in hexacyanoferrate complexes [34]. Similarly, the high-resolution XPS spectrum for ruthenium (Fig. 3C) shows peaks at 463.6 eV and 485.1 eV, attributed to Ru $3p_{3/2}$ and Ru $3p_{1/2}$, respectively. The observed peak positions and their 2:1 intensity ratio are characteristic of Ru in the +3 oxidation state [35]. These results confirm that ruthenium is present in the form of Ru^{3+} ions coordinated within the hexacyanoferrate framework. Taken together, the XPS results provide compelling evidence for the successful formation of a core–shell structure comprising Ru^{3+} and Fe^{3+} centers bridged by cyanide ligands. Based on the oxidation states and elemental composition, the chemical formula of the resulting complex can be proposed as $Ru[Fe(CN)_6]$, confirming the formation of the desired hexacyanoferrate architecture.

3.4. Electrochemical characterization of the SiO_2@RuHCF-NP modified electrode

Cyclic voltammetry (CV) was employed to study the electrochemical behaviour of SiO_2@RuHCF nanoparticle-modified electrodes. Fig. 4 presents the cyclic voltammograms of colloidal SiO_2 nanoparticles coated on PIGE, ferrocyanide over SiO_2 on PIGE, and SiO_2@RuHCF-modified PIGE electrodes, recorded in 0.1 M KCl at a scan rate of 50 mV s^{-1}. As shown, the bare graphite electrode (curve a) exhibits no voltammetric response. In contrast, the SiO_2–ferrocyanide-modified PIGE (curve b) shows a noticeable increase in background current along with broad redox peaks. For the SiO_2@RuHCF-modified electrode (curve c), well-defined redox peaks with significantly higher current are observed at 0.657 V and 0.586 V, corresponding to the Ru(III)–Fe(II)/Ru(III)–Fe(III) redox couple, consistent with previous findings by Chen et al. [36]. The formal potential, calculated as (Epc + Epa)/2, was found to be 0.621 V. The increased current is attributed to the formation of an inorganic polymeric shell over the colloidal silica particles. The SiO_2@RuHCF-modified PIGE electrode exhibited excellent stability. To assess its electrochemical durability, the electrode was subjected to 150 continuous potential cycles from −0.4 V to 1.2 V at 50 mV s^{-1} in 0.1 M KCl, with no significant decline in current observed. Furthermore, the chemically modified electrode demonstrated excellent shelf life, retaining 98 % of its initial activity after more than four months of storage in electrolyte solution.

3.5. Electrocatalytic reduction of riboflavin at the modified electrode

To study the electrocatalytic activity of the modified electrode with core-shell assembly towards the reduction of riboflavin (Vitamin B_2 or VB_2) cyclic voltammetric experiments have been carried out with the bare and modified electrode in presence of VB_2. The corresponding results are shown in Fig. 5. The curves (a and c) shows the CV of the bare and modified electrode. Negligible amount of current was observed in the presence of 9.25×10^{-5} M VB_2 at bare electrode surface (curve c). The peaks are attributed to the redox reactions of SiO_2@RuHCF, which is present on the PIGE and curve (d) shows the reduction of 9.25×10^{-5} M VB_2 with SiO_2@RuHCF NP modified electrode. It is seen that in presence of VB_2, the cathodic current increased to a large extent compared to the bare electrode (curve d), demonstrating a strong electrocatalytic effect. The redox peaks observed in the absence of VB_2 are attributed to the Fe^{3+}/Fe^{2+} and Ru^{3+}/Ru^{2+} redox couples of the RuHCF shell anchored on the SiO_2 core. Upon addition of VB_2, a substantial enhancement in cathodic current is observed at more negative potentials corresponding to the reduction of riboflavin. Although the reduction potential of VB_2 is significantly more negative than the intrinsic redox potentials of the Fe/Ru sites, the enhanced catalytic performance arises from an indirect electrocatalytic mechanism. The RuHCF shell acts as an efficient electron-transfer mediator, facilitating rapid charge transport between the electrode surface and riboflavin molecules once the applied potential is sufficiently negative to drive VB_2 reduction. The porous core–shell architecture increases the local concentration of VB_2 near the electrode surface and provides abundant redox-active sites, thereby lowering the kinetic barrier for electron transfer and accelerating the reduction process. This synergistic effect leads to a marked increase in cathodic current despite the non-overlapping redox potentials. Under optimized experimental conditions, the reduction peak current exhibited a linear relationship with VB_2 concentrations in the range of 4.3×10^{-6} to 2.6×10^{-3} M, with a detection limit of 1.4×10^{-7} M (S/N = 3). The electrocatalytic property of the modified electrode is dependent on several controllable parameters such as electrolyte, temperature, applied potential, pH, etc. The proposed electrocatalytic mechanism for VB_2 reduction at the SiO_2@RuHCF NP–modified electrode is illustrated in Scheme 2.

The effect of solution pH on the electrochemical behaviour of the RuHCF modified electrode in presence of 1.7×10^{-4} M VB_2 was investigated by CV at various pHs containing 0.1 M KCl as supporting electrolyte. The cyclic voltammetric results indicated that the electrochemical responses of the modified electrode were not much affected and a gradual increase of peak current was found in the pH range 3–5 (Fig. 6). The peak current was maximum at pH 7.0 and then it decreases as expected due to the hydroxylation of the mediator. Thus, an optimum pH of 7.0 was chosen for further experiments.

Hydrodynamic voltammetry was conducted to investigate the electrocatalytic behaviour of the SiO_2@RuHCF nanoparticle-modified

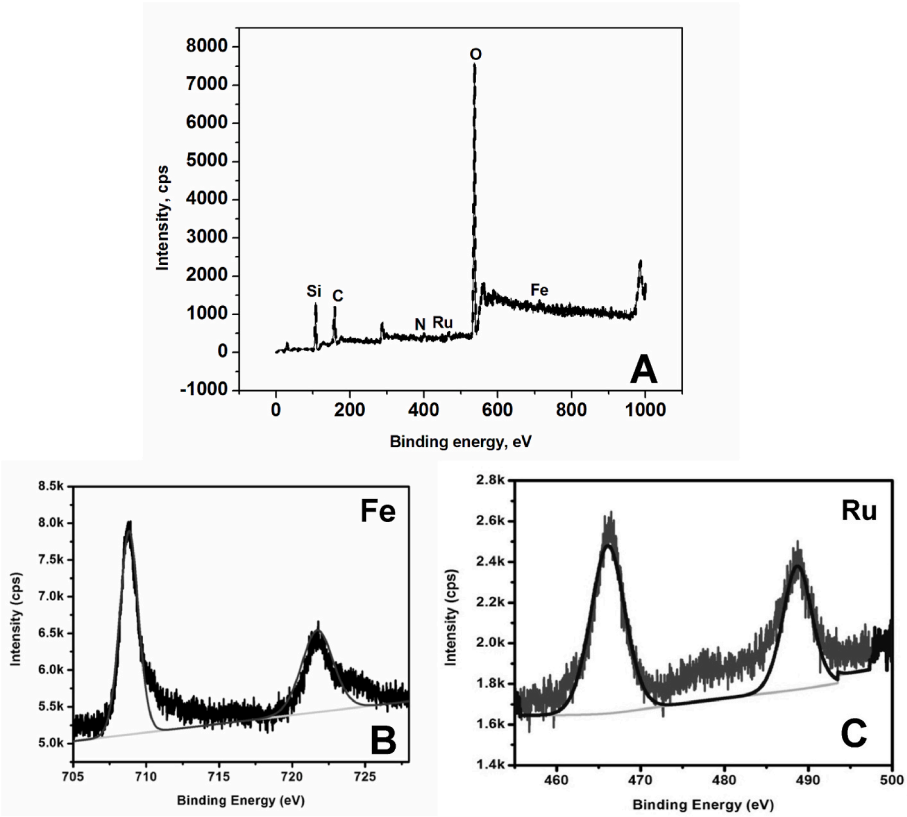

Fig. 3. XPS of SiO_2@RuHCF NP (a) Survey scan (b) 2p3/2 and 2p1/2 of Fe (III) and (c) 3p3/2 and 3p1/2 of Ru(III).

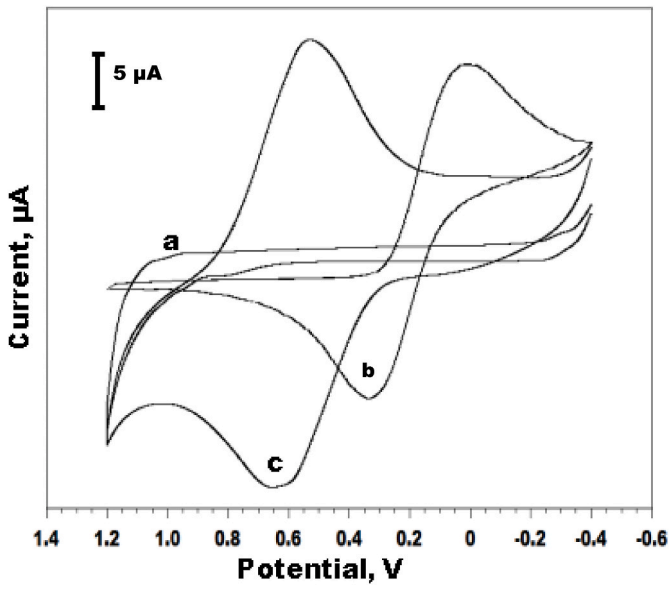

Fig. 4. Cyclic voltammograms of (a) colloidal SiO_2 NP coated on PIGE (b) ferrocyanide coated SiO_2 NP on PIGE (c) SiO_2@RuHCF-NP modified electrode in 0.1 M KCl; Scan rate 20 mV s^{-1}.

electrode under dynamic conditions and to determine the optimal operating potential for amperometric measurements. During the study, the working electrode potential was incrementally increased under constant stirring, and the resulting steady-state current was recorded and plotted against the applied potential. The bare electrode exhibited an almost negligible response, whereas the modified electrode showed a pronounced increase in current for the reduction of riboflavin (VB_2), as illustrated in Fig. 7. The current begins to rise from −0.5 V, indicating that a potential of −0.7 V or more negative can be applied for the electrocatalytic reduction of VB_2 in flow systems. To evaluate the performance of the modified electrode as an amperometric detector for VB_2 determination, chronoamperometric measurements were conducted in 0.1 M KCl. Based on the hydrodynamic voltammetry results, a potential of −0.7 V was selected. Fig. 8 presents a typical amperogram recorded at the modified electrode, showing a clear increase in current with successive additions of 9×10^{-5} M VB_2. The inset of Fig. 8 displays the corresponding calibration plot, which reveals a good linear relationship between peak current and VB_2 concentration over the range of 9×10^{-5} to 11.2×10^{-4} M, with a correlation coefficient of 0.9979. The relative standard deviation (RSD) for ten determinations was 2.5 %, confirming good reproducibility of the sensor.

Pulse voltammetric techniques such as differential pulse voltammetry (DPV) method were used to determine the concentration of riboflavin in standard samples. DPVs of VB_2 at SiO_2@RuHCF NP modified electrode at various concentrations are shown in Fig. 9. As seen from Fig. 9, DPV cathodic peak currents increased linearly with VB_2 concentration. The DPV calibration curve of VB_2 had a linear working range of 18×10^{-6}–14×10^{-4} M with a detection limit of 9.08×10^{-7} M VB_2 (S/N = 3) (Fig. 9). The correlation coefficient is 0.9955. The voltammetric detection with SiO_2@RuHCF NP modified electrode was very stable and R.S.D. (95 % confidence interval). The mechanism of electrocatalytic reduction of VB_2 at SiO_2@RuHCF-NPs modified electrode is given in Scheme 2 which is in accordance with the earlier report [34]. The immobilized RuHCF nanoparticles, initially in the oxidized state on the electrode surface, are reduced at the applied potential. The reduced form of the mediator subsequently reduces riboflavin in solution and is itself reoxidized. The regenerated oxidized form of the hexacyanoferrate nanoparticles is then reduced again at the electrode surface, producing a measurable reduction current. This cyclic process of analyte reduction and mediator regeneration continues, thereby amplifying the reduction

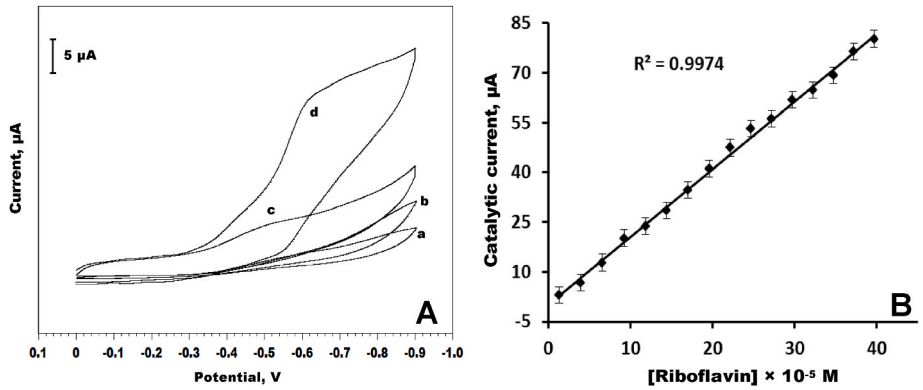

Fig. 5. (A) Cyclic voltammograms of (a) bare electrode (b) bare electrode in presence of 9.25×10^{-5} M riboflavin (c) SiO_2@RuHCF NP modified electrode (d) SiO_2@RuHCF NP modified electrode in presence of 9.25×10^{-5} M riboflavin in 0.1 M KCl; Scan rate: 50 mV s^{-1}. (B) Corresponding calibration curve.

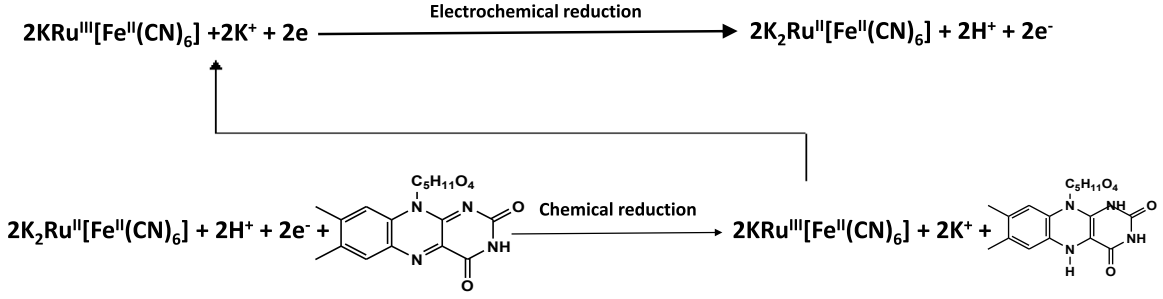

Scheme 2. Electrocatalytic reduction of VB_2 at the SiO_2@RuHCF-NPs modified electrode.

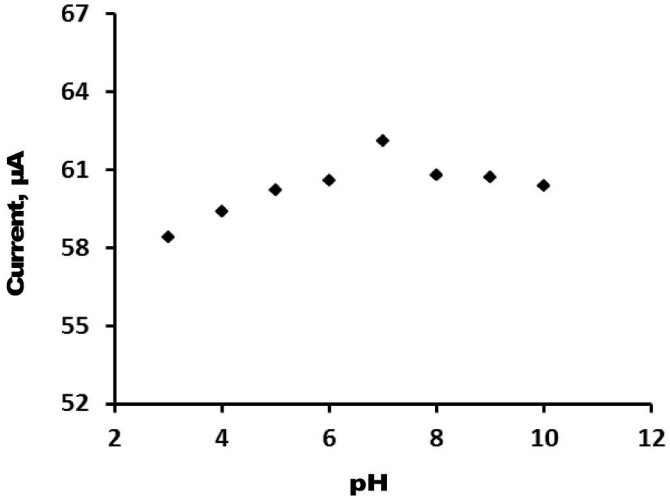

Fig. 6. Effect of pH versus peak current of SiO_2@RuHCF-NPs modified electrode in the presence of 1.7×10^{-4} M of riboflavin in 0.1 M KNO_3 at 50 mV s^{-1}.

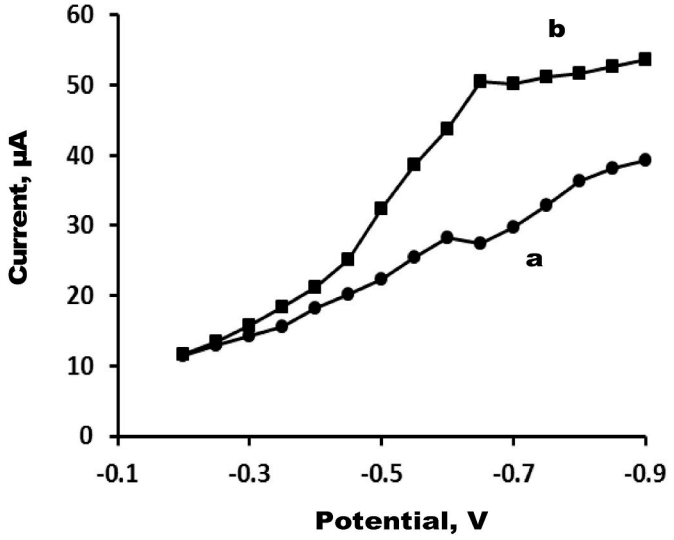

Fig. 7. Hydrodynamic voltammograms of (a) surface modified SiO_2@RuHCF-NPs electrode and (b) with 1.2×10^{-4} M riboflavin in 0.1 M KCl; Stirring rate 300 rpm.

current and enhancing the electrocatalytic response of the system.

3.6. Interference study

The selectivity of the SiO_2@RuHCF-NPs modified electrode for the determination of riboflavin (RF) was evaluated through interference studies using cyclic voltammetry. The current response for 10 mM RF was recorded in the presence of common inorganic ions such as Fe^{3+}, Mg^{2+}, Na^{+}, K^{+}, Ca^{2+}, NO_3^-, and SO_4^{2-} (each at 100-fold excess), as well as physiological interferents like ascorbic acid (AA) and uric acid (UA) at 50-fold excess, there was no significant variation in the cyclic voltammetry response was observed under these conditions, indicating negligible interference. These results demonstrate the high selectivity of the SiO_2@RuHCF-NPs modified electrode towards RF, even in the presence of potentially competing species commonly found in biological and environmental samples.

3.7. Stability and reproducibility

The long-term stability of the modified electrode toward VB_2

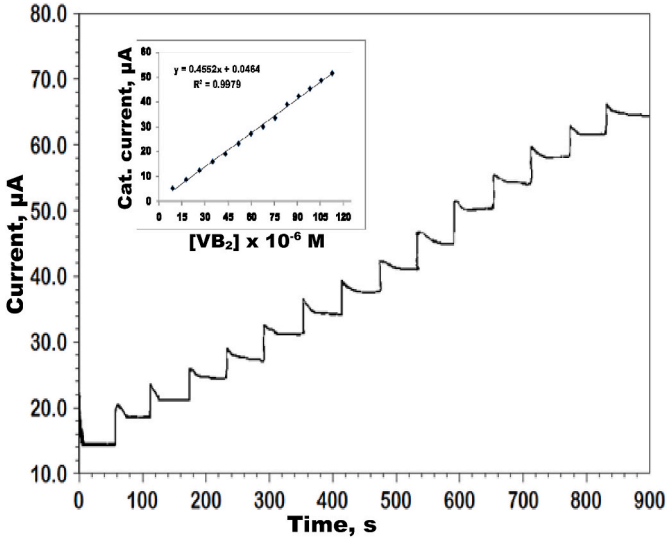

Fig. 8. Amperometric signals obtained during successive increments of 9 × 10^{-5} M VB_2 in 0.1 M KCl using the applied potential of −650 mV. Inset: Corresponding calibration curve.

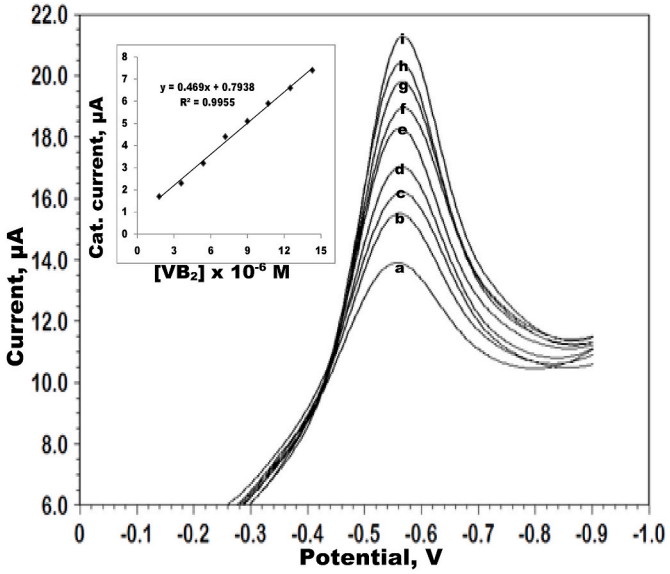

Fig. 9. Differential pulse voltammograms of SiO_2@RuHCF-NPs modified electrode at different concentrations of riboflavin where a-i corresponds to 0, 0.018, 0.036, 0.054, 0.072, 0.09, 0.108, 0.126, 0.144, 0.162, 0.18 mM of riboflavin in 0.1 M KCl. Inset: Calibration plot of VB_2.

detection was evaluated by monitoring its current response over a period of 60 days using a VB_2 concentration of 2.7 × 10^{-4} M. Measurements were taken at regular intervals of 5 days. As shown in Fig. 10, the electrode exhibited only a marginal decrease in current, with a loss of approximately 2–3 % relative to its initial response. This minimal change highlights the excellent stability and durability of the modified electrode for the electrochemical detection of VB_2. In addition to long-term stability, the short-term response of the electrode was also investigated. The current response was recorded over a 3 h period at 30 min intervals using 1.2 × 10^{-4} M VB_2 (inset of Fig. 10). The results indicated that the electrode maintained a highly stable and consistent response throughout the duration of the experiment, further confirming its reliability for practical applications.

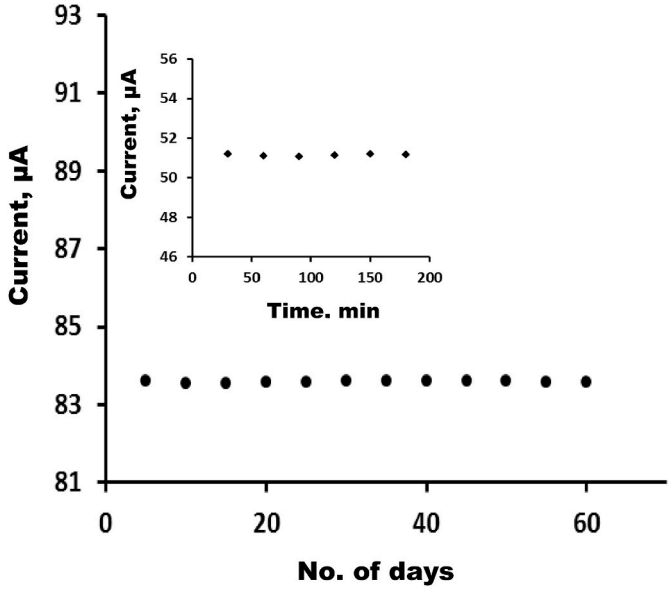

Fig. 10. Long-term stability response of the SiO_2@RuHCF-NPs modified electrode towards the reduction of 2.7 × 10^{-4} M of riboflavin; Inset: Current response of modified electrode for 1.2 × 10^{-4} M of riboflavin versus time in minutes.

3.8. Oxygen evolution reaction (OER) performance

It is well established that a high-performance OER electrocatalyst typically features a low onset potential, a reduced overpotential at a current density of 10 mA cm^{-2}, and the ability to deliver a higher current density at a given potential. To evaluate the OER electrocatalytic activity of the as-synthesized SiO_2@RuHCF-NPs modified electrode, linear sweep voltammetry (LSV) measurements were carried out in 1.0 M KOH electrolyte using a conventional three-electrode setup at a scan rate of 5 mV s^{-1}. The corresponding LSV curves are presented in Fig. 11A. The SiO_2@RuHCF-NPs modified electrode demonstrates significantly improved electrocatalytic performance compared to the bare electrode. Specifically, the hybrid catalyst exhibits a markedly lower onset potential of 560 mV versus the reversible hydrogen electrode (RHE), in contrast to 870 mV observed for the unmodified (bare) electrode. Furthermore, at a current density of 10 mA cm^{-2}, the SiO_2@RuHCF-NPs electrode shows a substantially reduced overpotential, along with a higher current density at the same applied potential. These enhancements in OER activity can be attributed to the synergistic interplay between Ru and Fe species within the Prussian blue analogue framework supported on the SiO_2 matrix. The lower onset potential and improved current response underscore the superior catalytic behavior of the SiO_2@RuHCF-NPs hybrid structure, confirming its potential as an efficient electrocatalyst for water oxidation reactions. In future studies will systematically vary the SiO_2 core size to understand its impact on ECSA and overall catalytic activity.

Tafel plots for SiO_2@RuHCF-NPs hybrid were recorded and compared with those of the bare electrode to evaluate their electrocatalytic performance toward the OER. Key kinetic parameters, including overpotential (η, in mV), current density (j, in mA cm^{-2}), and Tafel slope (in mV dec^{-1}), were used to assess the catalytic activity. As shown in Fig. 11B, the SiO_2@RuHCF NPs exhibit a Tafel slope of 107 mV dec^{-1}, which is significantly lower than the 405 mV dec^{-1} observed for the bare graphite electrode under identical experimental conditions. This reduction in Tafel slope by 300 mV dec^{-1} indicates enhanced OER kinetics. The improved electrocatalytic activity of the SiO_2@RuHCF NP-modified electrode is attributed to the synergistic effect of the mixed oxides of Ru and Fe derived from the SiO_2@RuHCF nanostructures.

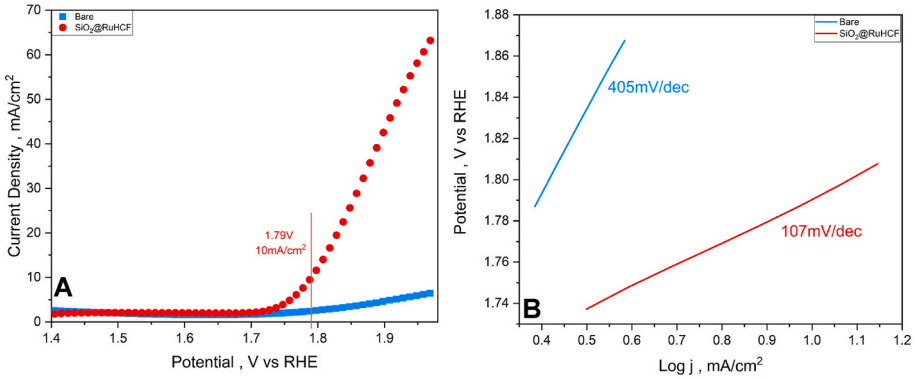

Fig. 11. LSV curves of bare and SiO_2@RuHCF-NPs at 5 mV s^{-1}, (B) Tafel plots of bare and SiO_2@RuHCF-NPs.

4. Conclusion

In this work, we successfully synthesized a novel inorganic oxide/polymer core-shell SiO_2@RuHCF-NPs and designed as an electrochemical sensor for riboflavin. On the basis of the morphology studies colloidal SiO_2 core can be directly coated with RuHCF to form a well-defined core/shell nanostructure. It provides an excellent electron transfer efficiency and large specific surface area with rich electroactive sites resulting in improved sensitivity and wide detection range toward electrocatalytic reduction of riboflavin. The above results suggest that the proposed sensor can be used as amperometric sensor for the determination of riboflavin. Furthermore, the SiO_2@RuHCF-NPs modified electrode demonstrated outstanding performance as an electrocatalyst for the OER, with a significantly reduced onset potential, lower overpotential at 10 mA cm^{-2}, and a much smaller Tafel slope compared to the bare electrode. These improvements highlight the synergistic effect of Ru and Fe within the Prussian blue analogue framework supported on the SiO_2 matrix. The dual functionality of the SiO_2@RuHCF hybrid showing both high sensitivity for riboflavin detection and excellent OER catalytic activity, suggests its promising potential in biosensing and energy-related applications.

CRediT authorship contribution statement

S. Anuja: Methodology, Investigation, Data curation, Conceptualization. **J.A.F.C.R. Rodrigues:** Software, Data curation. **R. Suresh Babu:** Writing – review & editing, Writing – original draft, Visualization, Validation, Project administration, Formal analysis. **A. Kosiha:** Software, Formal analysis, Data curation. **A.L.F. de Barros:** Supervision, Resources, Project administration.

Declaration of competing interest

The authors declare that they have no known competing financial interests or personal relationships that could have appeared to influence the work reported in this paper.

Acknowledgments

J.A.F.C.R. Rodrigues thanks CAPES FUC-01 for the scholarship. Dr. R.S. Babu thanks FAPERJ for the postdoctoral senior fellowship (E-26/203.465/2023). Prof. A.L.F. de Barros acknowledges financial support from Brazilian funding agencies, including the Conselho Nacional de Desenvolvimento Científico e Tecnológico (CNPq; Productivity Fellowship No. 307418/2021-9), Financiadora de Estudos e Projetos (FINEP) (1455/24), the Fundação de Amparo à Pesquisa do Estado do Rio de Janeiro (FAPERJ; Grants E/26-210.801/2021, E-26/200.320/2023, E-26/201.622/2023, E-26/204.934/2024, and E-26/210.836/2025), and the Coordenação de Aperfeiçoamento de Pessoal de Nível Superior (CAPES; Finance Code 001).

References

[1] R.G. Chaudhuri, S. Paria, Chem. Rev. 112 (2012) 2373–2433.
[2] M.B. Gawande, A. Goswami, T. Asefa, H. Guo, A.V. Biradar, D.-L. Peng, R. Zboril, R. S. Varma, Chem. Soc. Rev. 44 (2015) 7540–7590.
[3] C.F. Jones, L. Resina, F.C. Ferreira, P.S. Alberte, T. Esteves, J. Phys. Chem. C 128 (2024) 11083–11100.
[4] A.A. Nayl, A.I. Abd-Elhamid, A.A. Aly, S. Bräse, RSC Adv. 12 (2022) 13706–13726.
[5] H. Farmanbordar, M.S. Amini-Fazl, R. Mohammadi, J. Drug Deliv. Sci. Technol. 66 (2021) 102896.
[6] L.M. Samyn, R.S. Babu, R. Vinodh, R. Vivekananth, D.B. Haddad, A.L.F. de Barros, Diam. Relat. Mater. 144 (2024) 111017.
[7] R.S. Babu, P. Prabhu, S.S. Narayanan, J. Solid State Electrochem. 20 (2016) 1575–1583.
[8] R.O. Kadara, A.G. Fogg, B.G.D. Haggett, B.J. Birch, J. Agric. Food Chem. 57 (2009) 804.
[9] T. Brody, Nutritional Biochemistry, academic press, London, 1999, p. 609.
[10] P. Vinas, N. Balsalobre, C.L. Erroz, M.H. Cordoba, J. Agric. Food Chem. 52 (2004) 1789.
[11] C. Zhang, H. Qi, Anal. Sci. 18 (2002) 819.
[12] X.-M. Wang, H.Y. Chen, Spectrochim. Acta 51 (1996) 599.
[13] V.V. Shumyantseva, T.V. Bulko, N.A. Petushkoya, N.F. Samenkova, G. P. Kuznetsova, A.I. Archakov, J. Inorg. Biochem. 98 (2004) 365.
[14] L.S. Anisimova, E.V. Mikheeva, V.F. Slipchenko, J. Anal. Chem. 56 (2001) 658.
[15] A.A. Ahmed, B. Hou, H.S. Chavan, Y. Jo, S. Cho, J. Kim, S.M. Pawar, S. Cha, A. I. Inamdar, H. Kim, H. Im, Small 14 (2018) 1800742.
[16] Y.M. Chai, X.Y. Zhang, J.H. Lin, J.F. Qin, Z.Z. Liu, J.Y. Xie, B.Y. Guo, Z. Yang, B. Dong, Int. J. Hydrogen Energy 44 (2019) 10156–10162.
[17] X.L. Xiong, C. You, Z.A. Liu, A.M. Asiri, X.P. Sun, ACS Sustain Chem. Eng. 6 (2018) 2883–2887, 2018.
[18] S.J. Chao, Q.Y. Xia, G. Wang, X.Y. Zhang, Int. J. Hydrogen Energy 44 (2019) 4707–4715.
[19] X.J. Wu, B.M. Feng, W. Li, Y.L. Niu, Y.N. Yu, S.Y. Lu, C.Y. Zhong, P.Y. Liu, Z. Q. Tian, L. Chen, W.H. Hu, C.M. Li, Nano Energy 62 (2019) 117–126.
[20] T.T. Liu, L.S. Xie, J.H. Yang, R.M. Kong, G. Du, A.M. Asiri, X.P. Sun, L. Chen, Chemelectrochem 4 (2017) 1840–1845.
[21] K.L. Yan, J.Q. Chi, J.Y. Xie, B. Dong, Z.Z. Liu, W.K. Gao, J.H. Lin, Y.M. Chai, C. G. Liu, Renew. Energy 119 (2018) 54–61.
[22] Z.C. Wang, H.L. Liu, R.X. Ge, X. Ren, J. Ren, D.J. Yang, L.X. Zhang, X.P. Sun, ACS Catal. 8 (2018) 2236–2241.
[23] X.Q. Du, Q.Z. Shao, X.S. Zhang, Int. J. Hydrogen Energy 44 (2019) 2883–2888.
[24] T. Huang, Y. Chen, J.M. Lee, Small 13 (2017) 1702753.
[25] Z.Q. Wang, X. Ren, L. Wang, G.W. Cui, H.J. Wang, X.P. Sun, Chem. Commun. 54 (2018) 10993–10996.
[26] S. Wang, P. He, Z.W. Xie, L.P. Jia, M.Q. He, X.Q. Zhang, F.Q. Dong, H.H. Liu, Y. Zhang, C.X. Li, Electrochim. Acta 296 (2019) 644–652.
[27] B.M. Hunter, H.B. Gray, A.M. Muller, Chem. Rev. 116 (2016) 14120–14136.
[28] D.L. Zhang, H.Y. Mou, F. Lu, C.X. Song, D.B. Wang, Appl. Catal. B Environ. 254 (2019) 471–478.
[29] W. Stober, A. Finkh, J. Colloid Interface Sci. 26 (1968) 62.
[30] S. Heli, S. Majdi, N. Sattarahmady, Sensor. Actuator. B 145 (2010) 185.
[31] F. Scholz, B. Lange, Trends Anal. Chem. 11 (1992) 359.
[32] R. Vivekananth, R.S. Babu, R. Atchudan, Y. Sasikumar, A.L.F. de Barros, R. Kalaivani, Synth. Met. 311 (2025) 117829.
[33] T. Lopez, M. Villa, R. Comez, J. Phys. Chem. 95 (1991) 1690.
[34] J.T. Kloprogge, Appl. Sci. 15 (2025) 1318.
[35] A. Cano, L. Reguera, M. Avila, D. Velasco-Arias, E. Reguera, Eur. J. Inorg. Chem. (2020) 137–145.
[36] S.-M. Chen, M.-F. Lu, K.-C. Lin, J. Electroanal. Chem. 579 (2005) 163.